



The equivalent parallelogram and parallelepiped, and their application to stabilized finite elements in two and three dimensions

M. Küssner, B.D. Reddy *

*Centre for Research in Computational and Applied Mechanics, University of Cape Town, PD Hahn Building,
7701 Rondebosch, South Africa*

Received 10 November 1999

Abstract

A new class of quadrilateral and hexahedral elements (four- and eight-noded in two and three dimensions, respectively) is presented. These elements are obtained by combining the concept of the equivalent parallelogram for plane problems, and the equivalent parallelepiped for three-dimensional problems, with the notion of incompatible modes. A key feature of the new elements is that integration of the element stiffness matrices is carried out using one-point integration. The use of affine-equivalent elements (parallelograms and parallelepipeds) permits a closed-form eigenvalue analysis which includes the incompatible modes, and a stabilization procedure based on the eigenvalue analysis ensures the full rank of the stiffness matrix. Numerical results for problems in elasticity and plasticity indicate equivalent or superior performance of the new elements, when compared with various elements based on enhanced strains or incompatible modes. © 2001 Elsevier Science B.V. All rights reserved.

Keywords: Equivalent parallelogram; Equivalent parallelepiped; Incompatible modes; Stabilization

1. Introduction

The bilinear four-noded quadrilateral and trilinear eight-noded hexahedral elements are widely used in the finite element analysis of problems arising in solid mechanics. Unfortunately, use of the simple bi- or trilinear basis functions in displacement formulations leads to poor performance in bending-dominated situations, and in problems involving incompressibility or near-incompressibility.

A wide range of procedures have been proposed for resolving this difficulty. One commonly used remedy is that based on a combination of underintegration plus stabilization (see, for example, the work of [5,6]). The great advantage of this approach is its efficiency, in that only a single integration point is used. However, the components of the stabilization matrix are not uniquely defined in the case of non-affine elements (that is, elements which are not parallelograms in two dimensions or parallelepipeds in three), due to the fact that it is not possible to evaluate the eigenvalues of the stiffness matrix without an inappropriate amount of effort.

Stabilization by means of novel underintegration schemes is the subject of [10]. Integration over a quadrilateral is carried out numerically by subdividing the element into two triangles, and by using one-point integration on each triangle. The method has been proven to be robust and efficient.

* Corresponding author. Tel.: +1-27-21-650-2711; fax: +1-27-21-650-2710.
E-mail address: bdr@maths.uct.ac.za (B.D. Reddy).

Another popular approach is that associated with the enrichment or enhancement of the strain or stress field by the addition of carefully chosen basis functions. The key work dealing with enhanced strain formulations is [14]; in this approach the enhanced strain field is condensed out at element level, leading to a modified stiffness matrix.

The assumed stress approach [9] leads to a formulation very similar to that based on enhanced strains, and in fact the two are equivalent in certain circumstances [1]. Even the previously mentioned underintegrated elements with additional stabilization can be derived from enhanced strain elements for certain element shapes [8], so that a clear line cannot always be drawn between these methods. This holds particularly for affine elements.

It has been shown in [14] that any enhanced strain field has to fulfill certain conditions in order to ensure that the method is stable and consistent. The method of incompatible modes fulfills this condition for affine elements, while the modification due to Taylor ensures that the condition is fulfilled generally. For the enhanced strain method this condition is fulfilled readily by an appropriate choice of basis functions. Reddy and Simo [11] have examined this and other conditions in a study of the convergence of the method.

But still, for the enhanced strain element, the quality of approximations for arbitrary elements declines with increase in distortion. The approach that is complete to order two on the master element suffers a lack of completeness in physical space as the higher order enhanced strain field gets mapped from the master to the actual element. The key problem here is that the Jacobian matrix is non-constant. Nevertheless, these elements are convergent, as the study by Arunakirinathar and Reddy [3] has shown, and numerous computational tests have confirmed.

It follows that all the different element formulations are concerned with improving element performance in the case of non-affine elements. In this paper an alternative approach is taken. Rather than overcoming the problems of distortion by adding new modes, the geometry of the element is adapted to accommodate the modes that are used naturally with affine elements. More precisely, the arbitrary element is replaced by the affine element that is closest to it, in a manner that can be made precise. Such an affine element is known as the equivalent parallelogram in two dimensions, and the equivalent parallelepiped in three.

It has been shown in [2] that the interpolation error obtained by using the equivalent parallelogram instead of the original distorted element is of the same order as that corresponding to the usual interpolation error. The element stiffness matrices associated with the equivalent elements are therefore admissible alternatives to the ‘exact’ stiffness matrices of the original elements, while at the same time they are far easier to construct.

In Section 2 the equivalent parallelogram and parallelepiped are introduced. Section 3 is the core of this work; here the connection between the enhanced strain (or incompatible modes) and stabilization methods is made in the context of an eigenvalue analysis, and the extension of the method to small strain plasticity is given (the successful application of this methodology in the context of hyperelasticity, and in three dimensions, has been presented in [12,13]). Then, in Section 4, some numerical results are presented, in which the performance of the new element is compared with that of other elements, in two and three dimensions. The concluding section discusses related and future work.

2. Geometrical properties

The notion of the equivalent parallelogram associated with a quadrilateral arises naturally when one seeks to define the parallelogram that is closest to the quadrilateral, closeness being defined in an appropriate manner. Assuming that such a parallelogram can be constructed, the quadrilateral can then be regarded as a perturbation of the original domain.

Likewise, in the three-dimensional case, one seeks to construct an equivalent parallelepiped which is closest to a given hexahedron, in a sense made precise.

For brevity we summarize the relevant details in the context of the equivalent parallelepiped. The reduction to two dimensions is straightforward, and details can be found in [2].

Suppose that we are given an eight-noded hexahedron; this element can be generated by a *trilinear* map from a cubic master element $\hat{\Omega} = (-1, 1)^3$, according to

$$\mathbf{x} = \sum_{A=1}^8 \mathbf{x}_A N_A, \tag{1}$$

where

$$N_A(\boldsymbol{\xi}) = \frac{1}{8} (1 + \xi_A \xi)(1 + \eta_A \eta)(1 + \zeta_A \zeta) \tag{2}$$

and in which $\boldsymbol{\xi}_A = (\xi_A, \eta_A, \zeta_A)$ ($A = 1, \dots, 8$) are the coordinates of the vertices of the master element. If we define $\mathbf{N} = [N_1 \dots N_8]^T$, then (2) becomes, in vector form,

$$\mathbf{N}(\boldsymbol{\xi}) = \frac{1}{2} \underbrace{(\mathbf{r} + \mathbf{g}_\xi \xi + \mathbf{g}_\eta \eta + \mathbf{g}_\zeta \zeta)}_{\text{affine part}} + \underbrace{(\mathbf{h}_1 \eta \zeta + \mathbf{h}_2 \zeta \eta + \mathbf{h}_3 \xi \zeta + \mathbf{h}_4 \xi \eta \zeta)}_{\text{non-affine part}}. \tag{3}$$

The vectors $\mathbf{r}, \mathbf{g}_\xi, \mathbf{g}_\eta, \mathbf{g}_\zeta$ are respectively the rigid body and stretching modes, while \mathbf{h}_A ($A = 1, \dots, 4$) are the bending modes; these are given by

$$\mathbf{r} = \frac{1}{4} \begin{pmatrix} 1 \\ 1 \\ 1 \\ 1 \\ 1 \\ 1 \\ 1 \\ 1 \end{pmatrix}, \quad \mathbf{g}_\xi = \frac{1}{4} \begin{pmatrix} -1 \\ 1 \\ 1 \\ -1 \\ -1 \\ 1 \\ 1 \\ -1 \end{pmatrix}, \quad \mathbf{g}_\eta = \frac{1}{4} \begin{pmatrix} -1 \\ -1 \\ 1 \\ 1 \\ -1 \\ -1 \\ 1 \\ 1 \end{pmatrix}, \quad \mathbf{g}_\zeta = \frac{1}{4} \begin{pmatrix} -1 \\ -1 \\ -1 \\ -1 \\ 1 \\ 1 \\ 1 \\ 1 \end{pmatrix}, \tag{4}$$

$$\mathbf{h}_1 = \frac{1}{4} \begin{pmatrix} 1 \\ -1 \\ 1 \\ -1 \\ 1 \\ -1 \\ 1 \\ -1 \end{pmatrix}, \quad \mathbf{h}_2 = \frac{1}{4} \begin{pmatrix} 1 \\ 1 \\ -1 \\ -1 \\ -1 \\ -1 \\ 1 \\ 1 \end{pmatrix}, \quad \mathbf{h}_3 = \frac{1}{4} \begin{pmatrix} 1 \\ -1 \\ -1 \\ 1 \\ -1 \\ 1 \\ 1 \\ -1 \end{pmatrix}, \quad \mathbf{h}_4 = \frac{1}{4} \begin{pmatrix} -1 \\ 1 \\ -1 \\ 1 \\ 1 \\ -1 \\ 1 \\ -1 \end{pmatrix}. \tag{5}$$

The equivalent parallelepiped is then simply defined to be the figure obtained using only the *affine part* of the map (3). The nodal coordinates $\bar{\mathbf{x}}_B$ of the parallelepiped are thus given by

$$\begin{pmatrix} \bar{\mathbf{x}}_1 \\ \bar{\mathbf{x}}_2 \\ \bar{\mathbf{x}}_3 \\ \bar{\mathbf{x}}_4 \\ \bar{\mathbf{x}}_5 \\ \bar{\mathbf{x}}_6 \\ \bar{\mathbf{x}}_7 \\ \bar{\mathbf{x}}_8 \end{pmatrix} = \frac{1}{4} \begin{pmatrix} 2 & 1 & 0 & 1 & 1 & 0 & -1 & 0 \\ & 2 & 1 & 0 & 0 & 1 & 0 & -1 \\ & & 2 & 1 & -1 & 0 & 1 & 0 \\ & & & 2 & 0 & -1 & 0 & 1 \\ & & & & 2 & 1 & 0 & 1 \\ & & & & & 2 & 1 & 0 \\ & & & & & & 2 & 1 \\ \text{s y m} & & & & & & & 2 \end{pmatrix} \begin{pmatrix} \mathbf{x}_1 \\ \mathbf{x}_2 \\ \mathbf{x}_3 \\ \mathbf{x}_4 \\ \mathbf{x}_5 \\ \mathbf{x}_6 \\ \mathbf{x}_7 \\ \mathbf{x}_8 \end{pmatrix}.$$

The shift from the arbitrary hexahedron to its equivalent parallelepiped can be written using alternating vectors \mathbf{k}_i . These vectors may be obtained by writing the map (1) from the master element to the hexahedron in the form

$$\mathbf{x} = \mathbf{F}(\boldsymbol{\xi}) = \sum_{A=1}^8 N_A(\boldsymbol{\xi}) \bar{\mathbf{x}}_A + \sum_{A=1}^8 N_A(\boldsymbol{\xi}) (\mathbf{x}_A - \bar{\mathbf{x}}_A) = \sum_{A=1}^8 N_A(\boldsymbol{\xi}) \bar{\mathbf{x}}_A + \mathbf{k}_1 \zeta \eta + \mathbf{k}_2 \eta \zeta + \mathbf{k}_3 \xi \zeta + \mathbf{k}_4 \xi \eta \zeta \tag{6}$$

in which

$$\begin{aligned}
 \mathbf{k}_1 &= \frac{1}{8} (+\mathbf{x}_1 - \mathbf{x}_2 + \mathbf{x}_3 - \mathbf{x}_4 + \mathbf{x}_5 - \mathbf{x}_6 + \mathbf{x}_7 - \mathbf{x}_8), \\
 \mathbf{k}_2 &= \frac{1}{8} (+\mathbf{x}_1 + \mathbf{x}_2 - \mathbf{x}_3 - \mathbf{x}_4 - \mathbf{x}_5 - \mathbf{x}_6 + \mathbf{x}_7 + \mathbf{x}_8), \\
 \mathbf{k}_3 &= \frac{1}{8} (+\mathbf{x}_1 - \mathbf{x}_2 - \mathbf{x}_3 + \mathbf{x}_4 - \mathbf{x}_5 + \mathbf{x}_6 + \mathbf{x}_7 - \mathbf{x}_8), \\
 \mathbf{k}_4 &= \frac{1}{8} (-\mathbf{x}_1 + \mathbf{x}_2 - \mathbf{x}_3 + \mathbf{x}_4 + \mathbf{x}_5 - \mathbf{x}_6 + \mathbf{x}_7 - \mathbf{x}_8).
 \end{aligned}
 \tag{7}$$

It is worth emphasizing that the volumes of the hexahedron and its equivalent parallelepiped are equal.

The reduction to the two-dimensional case is achieved by setting the coordinate ζ equal to zero, and by summing over $1, \dots, 4$ in (1). In this case the rigid body mode \mathbf{r} , constant gradient modes \mathbf{g}_ξ and \mathbf{g}_η , and the hourglass mode \mathbf{h} take the form

$$\mathbf{r} = \frac{1}{2} \begin{pmatrix} 1 \\ 1 \\ 1 \\ 1 \end{pmatrix}, \quad \mathbf{g}_\xi = \frac{1}{2} \begin{pmatrix} -1 \\ 1 \\ 1 \\ -1 \end{pmatrix}, \quad \mathbf{g}_\eta = \frac{1}{2} \begin{pmatrix} 1 \\ -1 \\ -1 \\ 1 \end{pmatrix}, \quad \mathbf{h} = \frac{1}{2} \begin{pmatrix} 1 \\ -1 \\ 1 \\ -1 \end{pmatrix}.
 \tag{8}$$

The equivalent parallelogram associated with a quadrilateral is illustrated in Fig. 1.

2.1. Convergence properties

An analysis of the equivalent parallelogram, carried out in [2], leads to various results that are of use in establishing the convergence of finite element approximations based on the four-noded quadrilateral. For example, let

$$\mathbf{x} = \bar{\mathbf{F}}(\boldsymbol{\xi}) = \bar{\mathbf{A}}\boldsymbol{\xi} + \bar{\mathbf{c}}
 \tag{9}$$

represent the affine map from the master element to the equivalent parallelogram; here $\bar{\mathbf{A}}$ and $\bar{\mathbf{c}}$ are respectively a constant matrix and vector. Then, if the length of the longer diagonal of the parallelogram is h , it can be shown that there exist positive constants c_i ($i = 1, \dots, 6$), independent of h , such that

$$\begin{aligned}
 c_1 h &\leq \|\bar{\mathbf{A}}\| \leq c_2 h, \\
 c_3 h &\leq \|\bar{\mathbf{A}}^{-1}\| \leq c_4 h, \\
 c_5 h^2 &\leq \|\det \bar{\mathbf{A}}\| \leq c_6 h^2.
 \end{aligned}
 \tag{10}$$

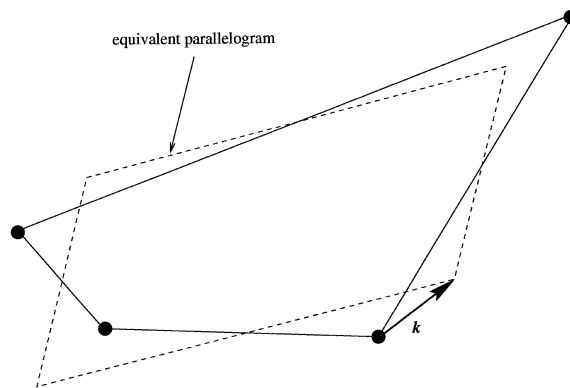


Fig. 1. The equivalent parallelogram.

These bounds allow one to obtain the interpolation error estimate for an arbitrary quadrilateral whose equivalent parallelogram corresponds to the map $\bar{\mathbf{F}}$, and it is shown in [2] that there exists a constant C , independent of h , such that

$$|u - \Pi u|_1 \leq Ch; \quad (11)$$

$|\cdot|_1$ is the H^1 – or energy seminorm and Πu represents the interpolate of a function $u \in H^2(\Omega)$, in the sense that the image of Π on the master element is a member of Q_1 , the space of bilinear functions.

In the same way it can be shown that if \mathbf{K} and $\bar{\mathbf{K}}$ are the stiffness matrices corresponding to the quadrilateral and its equivalent element, then the *consistency error* E , defined by

$$E = \|\mathbf{K} - \bar{\mathbf{K}}\|, \quad (12)$$

and which represents the error due to the replacement of quadrilaterals by their equivalent parallelograms, is bounded in the sense that

$$E \leq Ch$$

for some positive constant C . This error is of the same order as the interpolation estimate, so that the total finite element error remains one of order h . Similar results hold in the three-dimensional case. These error estimates are of course no guarantee that the use of equivalent elements will lead to an improvement in approximations – the estimates are, after all, asymptotic – but it will be shown in Section 4 that this approach does indeed give very satisfactory results, with a significant reduction in computational effort.

3. Incompatible modes and equivalence with underintegration plus stabilization

We begin by reviewing the incompatible modes formulation for a parallelogram and a parallelepiped; this formulation will then be transformed to an equivalent one based on one-point underintegration plus stabilization.

At this stage, it should be pointed out that the underintegrated stiffness matrices of the arbitrary quadrilateral and its equivalent parallelogram are identical. This becomes obvious if one bears in mind that the equivalent parallelogram represents the affine part of the mapping of an arbitrary quadrilateral, so that the constant part of the stiffness matrix of the arbitrary quadrilateral and its equivalent parallelogram are identical. The proposed method can therefore be understood in terms of the usual underintegration method where the properties of the equivalent parallelogram are used only to evaluate the stabilization factors analytically.

3.1. Parallelograms

We require various properties of an arbitrary parallelogram, shown in Fig. 2.

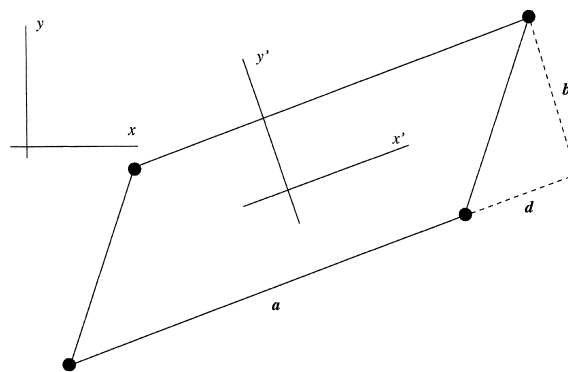


Fig. 2. Geometrical properties of the parallelogram.

If $(x'y')$ is a coordinate system with origin at the centroid, and the x' -axis parallel to one of the sides of the element, then the map from the master element to the parallelogram takes the form

$$x' = \frac{a}{2}\xi + \frac{d}{2}\eta \quad \text{and} \quad y' = \frac{b}{2}\eta, \quad (13)$$

where a, b and d are defined in Fig. 2. This map has the Jacobian matrix

$$\mathbf{J} = \frac{1}{2} \begin{pmatrix} a & d \\ 0 & b \end{pmatrix}. \quad (14)$$

For a problem in solid mechanics with displacement vector \mathbf{u} , we write the compatible part of the displacement in the form

$$\mathbf{u} = \sum_{A=1}^4 \mathbf{N}_A^T \hat{\mathbf{u}}_A, \quad \mathbf{v} = \sum_{A=1}^4 \mathbf{N}_A^T \hat{\mathbf{v}}_A, \quad (15)$$

where $\hat{\mathbf{u}}_A$ and $\hat{\mathbf{v}}_A$ are nodal values.

The derivatives are then found from (1) and (8) to be given by

$$\begin{pmatrix} \frac{\partial \mathbf{N}}{\partial x'} \\ \frac{\partial \mathbf{N}}{\partial y'} \end{pmatrix} = \mathbf{J}^{-T} \begin{pmatrix} \frac{\partial \mathbf{N}}{\partial \xi} \\ \frac{\partial \mathbf{N}}{\partial \eta} \end{pmatrix} = \begin{pmatrix} \frac{1}{a}(\mathbf{g}_\xi + \mathbf{h}\eta) \\ -\frac{d}{ab}(\mathbf{g}_\xi + \mathbf{h}\eta) + \frac{1}{b}(\mathbf{g}_\eta + \mathbf{h}\xi) \end{pmatrix}, \quad (16)$$

and the discrete strain field can be written as

$$\boldsymbol{\epsilon} = \mathbf{B}^T \mathbf{d}, \quad (17)$$

where \mathbf{d} is the nodal displacement vector: that is, $\mathbf{d} = (\hat{u}_1 \hat{v}_1 \hat{u}_2 \hat{v}_2 \hat{u}_3 \hat{v}_3 \hat{u}_4 \hat{v}_4)^T$. The matrix \mathbf{B} can be split into a constant part \mathbf{B}_0 and a linear part \mathbf{B}_1 , according to

$$\mathbf{B}^T = \underbrace{\mathbf{B}_0^T + \mathbf{B}_1^T}_{\text{constant}} = \frac{1}{ab} \begin{pmatrix} b\mathbf{g}_\xi^T & 0 \\ 0 & -d\mathbf{g}_\xi^T + a\mathbf{g}_\eta^T \\ -d\mathbf{g}_\xi^T + a\mathbf{g}_\eta^T & b\mathbf{g}_\xi^T \end{pmatrix} + \frac{1}{ab} \underbrace{\begin{pmatrix} b\mathbf{h}^T\eta & 0 \\ 0 & -d\mathbf{h}^T\eta + a\mathbf{h}^T\xi \\ -d\mathbf{h}^T\eta + a\mathbf{h}^T\xi & b\mathbf{h}^T\eta \end{pmatrix}}_{\text{linear in } \xi \text{ and } \eta}. \quad (18)$$

The incompatible modes. The basic idea of the method of incompatible modes is to enrich the approximation of the displacement field by adding the terms proposed in [16] and [17]. That is, we add to (15) the modes

$$\begin{pmatrix} \tilde{u} \\ \tilde{v} \end{pmatrix} = \begin{pmatrix} \varphi_1(1 - \xi^2) + \varphi_2(1 - \eta^2) \\ \varphi_3(1 - \xi^2) + \varphi_4(1 - \eta^2) \end{pmatrix}. \quad (19)$$

The derivatives in physical space are

$$\begin{aligned} \frac{\partial \tilde{u}}{\partial x'} &= -\frac{4}{a}\varphi_1\xi, & \frac{\partial \tilde{v}}{\partial x'} &= -\frac{4}{a}\varphi_3\xi, \\ \frac{\partial \tilde{u}}{\partial y'} &= \frac{4d}{ab}\varphi_1\xi - \frac{4}{b}\varphi_2\eta, & \frac{\partial \tilde{v}}{\partial y'} &= \frac{4d}{ab}\varphi_3\xi - \frac{4}{b}\varphi_4\eta, \end{aligned} \quad (20)$$

and the complete strain field is now

$$\boldsymbol{\epsilon} = \mathbf{B}^T \mathbf{d} + \mathbf{G}^T \boldsymbol{\varphi} \quad (21)$$

with the matrix \mathbf{G} given by

$$\mathbf{G}^T = -\frac{4}{ab} \begin{pmatrix} b\xi & 0 & 0 & 0 \\ 0 & 0 & -d\xi & a\eta \\ -d\xi & a\eta & b\xi & 0 \end{pmatrix}. \tag{22}$$

The degrees of freedom φ_i can be condensed out at element level to give

$$\boldsymbol{\varphi} = -\left[\int_{\Omega} \mathbf{G} \mathbf{D} \mathbf{G}^T d\Omega \right]^{-1} \left[\int_{\Omega} \mathbf{G} \mathbf{D} \mathbf{B}_1 d\Omega \right] \mathbf{d}, \tag{23}$$

in which \mathbf{D} is the elasticity matrix, so that the strain field can be written in the form

$$\boldsymbol{\epsilon} = (\mathbf{B}_0^T + \mathbf{B}_1^T) \mathbf{d} + \mathbf{G}^T \boldsymbol{\varphi} \equiv (\mathbf{B}_0^T + \mathbf{B}_*^T) \mathbf{d}. \tag{24}$$

An eigenvalue analysis. Since

$$\int_{-1}^1 \int_{-1}^1 \mathbf{B}_0^T \mathbf{D} \mathbf{B}_* \det[\mathbf{J}] d\xi d\eta = \int_{-1}^1 \int_{-1}^1 \mathbf{B}_*^T \mathbf{D} \mathbf{B}_0 \det[\mathbf{J}] d\xi d\eta = 0, \tag{25}$$

we may write the stiffness matrix in the decoupled form

$$\mathbf{K} = \mathbf{K}_0 + \mathbf{K}_* = \int_{-1}^1 \int_{-1}^1 \mathbf{B}_0^T \mathbf{D} \mathbf{B}_0 \det[\mathbf{J}] d\xi d\eta + \int_{-1}^1 \int_{-1}^1 \mathbf{B}_*^T \mathbf{D} \mathbf{B}_* \det[\mathbf{J}] d\xi d\eta, \tag{26}$$

where the matrix \mathbf{K}_* is defined by

$$\mathbf{K}_* = \frac{Eab^2}{3(b^2 + d^2)^2(1-\nu)(1+\nu)} \begin{pmatrix} \kappa \mathbf{h} \mathbf{h}^T & d \mathbf{h} \mathbf{h}^T \\ d \mathbf{h} \mathbf{h}^T & b \mathbf{h} \mathbf{h}^T \end{pmatrix}. \tag{27}$$

This is the rank two stabilization matrix for the plane strain problem; here

$$\kappa = \frac{b^4 + a^2 d^2 + 2b^2 d^2 + d^4}{a^2 b}. \tag{28}$$

Six of the eight eigenmodes arise from the constant part of the stiffness matrix \mathbf{K}_0 and are easily evaluated using one-point integration. The underintegrated element has to be stabilized in the usual way using the eigenvectors corresponding to the flexure modes; these are easily calculated from the linear part of the stiffness matrix (27) (see also [7]). The eigenmodes in the (x, y) coordinate system (see Fig. 2) are related to those in the x', y' system according to

$$\begin{aligned} \mathbf{e}_7^T &= \frac{1}{\sqrt{1 + \lambda_7^2}} [(\lambda_7 \cos \alpha + \sin \alpha) \mathbf{h}^T \quad (-\lambda_7 \sin \alpha + \cos \alpha) \mathbf{h}^T], \\ \mathbf{e}_8^T &= \frac{1}{\sqrt{1 + \lambda_8^2}} [(\lambda_8 \cos \alpha + \sin \alpha) \mathbf{h}^T \quad (-\lambda_8 \sin \alpha + \cos \alpha) \mathbf{h}^T]. \end{aligned} \tag{29}$$

With $\mathbf{K}_* = \lambda_7 \mathbf{e}_7 \mathbf{e}_7^T + \lambda_8 \mathbf{e}_8 \mathbf{e}_8^T$, Eq. (27) takes the form

$$\mathbf{K}_* = \begin{pmatrix} \epsilon_1 \mathbf{h} \mathbf{h}^T & \epsilon_2 \mathbf{h} \mathbf{h}^T \\ \epsilon_2 \mathbf{h} \mathbf{h}^T & \epsilon_3 \mathbf{h} \mathbf{h}^T \end{pmatrix}, \tag{30}$$

in which ϵ_i ($i = 1, 2, 3$) are expressed in terms of λ_7 , λ_8 and α . The same procedure has been presented for rectangular elements in [8].

The patch test. The approach given above converges to the exact solution by using the hourglass vectors \mathbf{h} for the stabilization of the underintegrated stiffness matrix. In the case of distorted elements, however, the patch test is not fulfilled. To avoid this undesirable aspect, the hourglass vector is replaced by the $\boldsymbol{\gamma}$ -vector (see, for example, [4,6]. The $\boldsymbol{\gamma}$ -vector has the form

$$\boldsymbol{\gamma} = \mathbf{h} - \frac{J_2}{J_0} \mathbf{g}_\xi - \frac{J_1}{J_0} \mathbf{g}_\eta \tag{31}$$

with the split of the determinant of the Jacobian matrix into a constant and two linear parts, that is,

$$J = \det \mathbf{J} = J_0 + J_1 \xi + J_2 \eta. \quad (32)$$

The coefficients are

$$\begin{aligned} J_0 &= a_1 b_3 - a_3 b_1, \\ J_1 &= a_1 b_2 - a_2 b_1, \\ J_2 &= a_2 b_3 - a_3 b_2 \end{aligned} \quad (33)$$

with

$$\begin{pmatrix} a_0 & b_0 \\ a_1 & b_1 \\ a_2 & b_2 \\ a_3 & b_3 \end{pmatrix} = \frac{1}{2} \begin{pmatrix} \mathbf{r}^T \\ \mathbf{g}_\xi^T \\ \mathbf{g}_\eta^T \\ \mathbf{h}^T \end{pmatrix} (\mathbf{x} \quad \mathbf{y}). \quad (34)$$

It can easily be seen that the γ -vector and the \mathbf{h} -vector are identical for the case of affine elements, for which the factors J_1 and J_2 vanish. With this inexpensive conversion of the \mathbf{h} -vector the patch test is fulfilled.

3.2. Stabilization with plasticity

The approach outlined above holds for linear and nonlinear problems. In the following the modifications necessary to treat small strain plasticity and large displacements is investigated. Results for hyperelastic problems have been presented in [12].

For a problem such as that involving both plasticity and large displacements, the conventional stiffness matrix will be modified as a result of both nonlinear material as well as geometric effects. Suppose that this matrix, obtained after suitable linearization, is denoted by \mathbf{K}^{nl} ; then \mathbf{K}^{nl} may also be decomposed into constant and linear parts: that is,

$$\mathbf{K}^{\text{nl}} = \mathbf{K}_o^{\text{nl}} + \mathbf{K}_*^{\text{nl}} = \sum_{n=1}^{\text{elem}} \left[\mathbf{K}_o^{\text{nl}} + \begin{pmatrix} \epsilon_1 \gamma \gamma^T & \epsilon_2 \gamma \gamma^T \\ \epsilon_2 \gamma \gamma^T & \epsilon_3 \gamma \gamma^T \end{pmatrix} \right] \quad (35)$$

while the residual becomes

$$\mathbf{R} = \sum_{n=1}^{\text{elem}} \left[\mathbf{R}_o + \begin{pmatrix} \epsilon_1 \gamma \gamma^T \mathbf{d}_x + \epsilon_2 \gamma \gamma^T \mathbf{d}_y \\ \epsilon_2 \gamma \gamma^T \mathbf{d}_x + \epsilon_3 \gamma \gamma^T \mathbf{d}_y \end{pmatrix} \right], \quad (36)$$

with \mathbf{d}_x and \mathbf{d}_y being the vectors of components of the displacement vector \mathbf{d} .

To achieve quadratic convergence in the application of Newton's method the tangent stiffness matrix has to be calculated from the linearization of the residual. In the proposed method, however, a consistent linearization cannot be given, as the scalars ϵ_i are themselves functions of the displacement: $\epsilon_i = \epsilon_i(\mathbf{d})$. Nevertheless, the method is interesting also for nonlinear problems because quadratic convergence can be achieved with constant ϵ_i . So, if the ϵ_i are updated only once at the beginning of a timestep, the results converge quadratically. It turns out that the frequency of updates of the stabilization factors has very little influence on the quality of the solution, so that updating once in a timestep is a reliable choice. The elements for nonlinear problems are again very fast as no inversion has to be carried out, even though the calculation of ϵ_i is more difficult as the material matrix becomes fully populated for nonlinear problems. Another major advantage is that associated with the number of history variables; there are at least 56 for a nonlinear plane enhanced strain element, whereas in the proposed method, the only history variables are the scalars ϵ_i and the stress history data at a single gauss point, giving a total of 9 history variables per element.

The calculation of the stabilization factors for a fully occupied material matrix is more difficult, and is presented in Appendix A.

3.3. Stabilization for the parallelepiped

The stabilization factors for the three-dimensional parallelepiped are calculated in a manner similar to that for the case of the parallelogram. To the usual quadratic approach of Wilson et al. [17] with 9 enhanced modes, 3 trilinear terms are added in order to prevent locking in the nearly incompressible limit. This enhancement method is comparable to the 12 enhanced modes that have been introduced by Simo et al. [15].

3.3.1. The compatible approach

We proceed as in the case of the parallelogram, and define a system of coordinates (x', y', z') with origin at the centroid of the parallelepiped, and with the $x'-y'$ plane parallel to one of the sides of the figure. Then the parallelepiped may be generated by a map from the master element $\hat{\Omega} = (-1, 1)^3$, according to

$$\begin{aligned} x' &= \frac{a}{2}\xi + \frac{d}{2}\eta + \frac{e}{2}\zeta, \\ y' &= \frac{b}{2}\eta + \frac{f}{2}\zeta, \\ z' &= \frac{c}{2}\zeta. \end{aligned} \tag{37}$$

Bearing in mind that the map to a parallelepiped is affine, with no bi- or tri-linear terms, the Jacobian matrix is constant, and is given by

$$\mathbf{J} = \frac{1}{2} \begin{pmatrix} a & 0 & 0 \\ d & b & 0 \\ e & f & c \end{pmatrix} \tag{38}$$

with determinant

$$\det[\mathbf{J}] = \frac{1}{8} abc. \tag{39}$$

From (4) and (5), the derivatives with respect to the coordinates of the master element are given by

$$\begin{aligned} \frac{\partial \mathbf{N}}{\partial \xi} &= \frac{1}{2} (\mathbf{g}_\xi + \mathbf{h}_1 \eta + \mathbf{h}_3 \zeta + \mathbf{h}_4 \eta \zeta), \\ \frac{\partial \mathbf{N}}{\partial \eta} &= \frac{1}{2} (\mathbf{g}_\eta + \mathbf{h}_1 \xi + \mathbf{h}_2 \zeta + \mathbf{h}_4 \xi \zeta), \\ \frac{\partial \mathbf{N}}{\partial \zeta} &= \frac{1}{2} (\mathbf{g}_\zeta + \mathbf{h}_2 \eta + \mathbf{h}_3 \xi + \mathbf{h}_4 \xi \eta), \end{aligned}$$

and the derivatives with respect to the (x', y', z') coordinate system, which follow from

$$\begin{pmatrix} \frac{\partial \mathbf{N}}{\partial x'} \\ \frac{\partial \mathbf{N}}{\partial y'} \\ \frac{\partial \mathbf{N}}{\partial z'} \end{pmatrix} = \mathbf{J}^{-T} \begin{pmatrix} \frac{\partial \mathbf{N}}{\partial \xi} \\ \frac{\partial \mathbf{N}}{\partial \eta} \\ \frac{\partial \mathbf{N}}{\partial \zeta} \end{pmatrix},$$

can easily be written in terms of the eigenvectors; thus we have

with the matrix \mathbf{G}^T being defined by

$$\mathbf{G}^T = \begin{pmatrix} \frac{-4\zeta}{a} & 0 & 0 & 0 & 0 & 0 & 0 & 0 & 0 & \frac{2\eta\zeta}{a} & \alpha_2 & \alpha_3 \\ 0 & 0 & 0 & \alpha_1 & \frac{-4\eta}{b} & 0 & 0 & 0 & 0 & \frac{2\eta\zeta}{a} & \alpha_2 & \alpha_3 \\ 0 & 0 & 0 & 0 & 0 & 0 & \alpha_4 & \frac{4\eta f}{bc} & \frac{-4\zeta}{c} & \frac{2\eta\zeta}{a} & \alpha_2 & \alpha_3 \\ \alpha_1 & \frac{-4\eta}{b} & 0 & \frac{-4\zeta}{a} & 0 & 0 & 0 & 0 & 0 & 0 & 0 & 0 \\ 0 & 0 & 0 & \alpha_4 & \frac{4\eta f}{bc} & \frac{-4\zeta}{c} & \alpha_1 & \frac{-4\eta}{b} & 0 & 0 & 0 & 0 \\ \alpha_4 & \frac{4\eta f}{bc} & \frac{-4\zeta}{c} & 0 & 0 & 0 & \frac{-4\zeta}{a} & 0 & 0 & 0 & 0 & 0 \end{pmatrix}, \quad (44)$$

and with

$$\begin{aligned} \alpha_1 &= \frac{4d\zeta}{ab}, \\ \alpha_2 &= \frac{2(- (d\eta\zeta) + a\zeta\zeta)}{ab}, \\ \alpha_3 &= \frac{2(\eta(- (be) + df)\zeta + a\zeta(b\eta - f\zeta))}{abc}, \\ \alpha_4 &= \frac{4(- (be) + df)\zeta}{abc}. \end{aligned}$$

As in the plane case the internal incompatible degrees of freedom $\boldsymbol{\varphi}$ may be condensed out at element level, to give (23), where the material matrix \mathbf{D} takes the form

$$\mathbf{D} = \begin{bmatrix} \lambda + 2\mu & \lambda & \lambda & 0 & 0 & 0 \\ \lambda & \lambda + 2\mu & \lambda & 0 & 0 & 0 \\ \lambda & \lambda & \lambda + 2\mu & 0 & 0 & 0 \\ 0 & 0 & 0 & \mu & 0 & 0 \\ 0 & 0 & 0 & 0 & \mu & 0 \\ 0 & 0 & 0 & 0 & 0 & \mu \end{bmatrix}, \quad (45)$$

λ and μ being the Lamé constants. The inversion of the 12×12 -matrix $\int_{\Omega} \mathbf{GDG}^T d\Omega$ can easily be carried out analytically as it breaks down into several submatrices with maximum dimension 3×3 . The strain field $\boldsymbol{\epsilon}$ is then given by (24), as before.

3.3.3. The stabilization matrix

The linear strain–displacement matrix \mathbf{B}_* can be expressed in terms of the four eigenvectors \mathbf{h}_i . Because of the mutual orthogonality of the eigenvectors, the stiffness matrix can be split into constant and linear parts: that is, we may write

$$\mathbf{K} = \mathbf{K}_o + \mathbf{K}_* = \int_{-1}^1 \int_{-1}^1 \int_{-1}^1 \mathbf{B}_o^T \mathbf{D} \mathbf{B}_o \det[\mathbf{J}] d\zeta d\eta d\zeta + \int_{-1}^1 \int_{-1}^1 \int_{-1}^1 \mathbf{B}_*^T \mathbf{D} \mathbf{B}_* \det[\mathbf{J}] d\zeta d\eta d\zeta. \quad (46)$$

The matrix \mathbf{K}_o can be easily obtained by one-point underintegration, so that the additional matrix \mathbf{K}_* can be regarded as the stabilization matrix.

The stabilization matrix \mathbf{K}_* is, in terms of the four vectors \mathbf{h}_i ,

$$\mathbf{K}_* = \sum_{i=1}^4 \sum_{j=1}^4 \begin{pmatrix} ev_{ij}(1, 1) \mathbf{h}_i \mathbf{h}_j^T & ev_{ij}(1, 2) \mathbf{h}_i \mathbf{h}_j^T & ev_{ij}(1, 3) \mathbf{h}_i \mathbf{h}_j^T \\ & ev_{ij}(2, 2) \mathbf{h}_i \mathbf{h}_j^T & ev_{ij}(2, 3) \mathbf{h}_i \mathbf{h}_j^T \\ & & ev_{ij}(3, 3) \mathbf{h}_i \mathbf{h}_j^T \end{pmatrix}, \quad (47)$$

(sym)

in which the terms ev_{ij} can be obtained analytically for a general element geometry and material law. Material nonlinearities can be accommodated in much the same way as was shown for the plane case. The analytical evaluation of the stabilization factors ensures a completely inversion-free evaluation of the element stiffness matrix.

3.3.4. A new element: Q1EP

Having constructed element stiffness matrices based on compatible modes in both two and three dimensions (Eqs. (30) and (47), respectively), we now return to the original problem of finding the stiffness matrix for an arbitrary quadrilateral or hexahedron. In line with the motivation given in the introduction and in Section 2.3, we choose as the stiffness matrix for the distorted element simply that associated with the corresponding equivalent parallelogram or parallelepiped. The resulting element is denoted by Q1EP (for Q1 with the enhanced parallelogram or parallelepiped).

4. Numerical examples

We give in this section a variety of examples in both two and three dimensions, in order to evaluate the performance of the elements proposed in this work. The performance of the new elements is compared against that of now-standard elements which have been enhanced in one way or another.

4.1. Plane problems

Example 1 (The two-element test). This standard benchmark problem is treated as one in plane strain, with $E = 70$ units and $\nu = 0.3$. The beam has length 10 units and height 2. Distortion is measured by the parameter a shown in Fig. 3. The loading is adjusted so as to give a unit vertical tip deflection in the undistorted case.

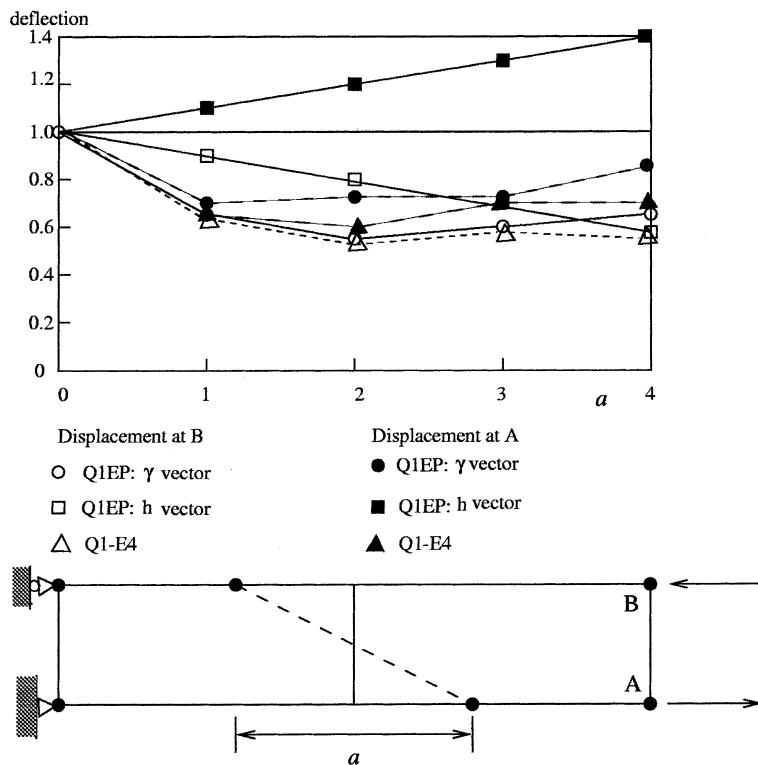


Fig. 3. The two-element test.

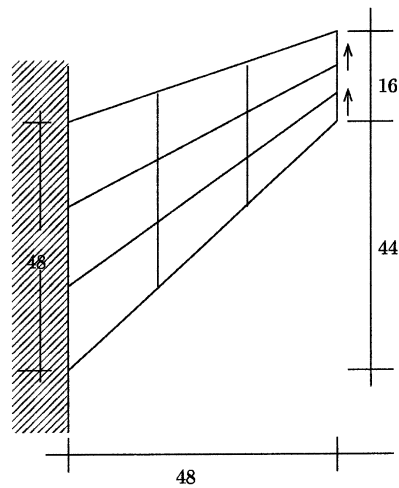
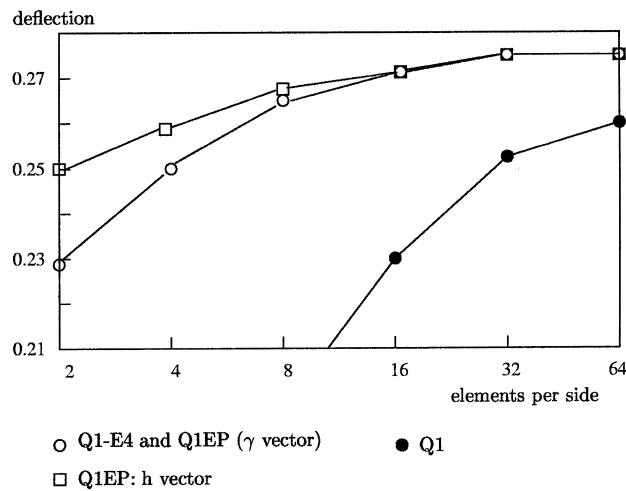


Fig. 4. Cook's membrane problem.

Fig. 3 shows graphs of variation in tip deflection with distortion. Results for the Q1EP element are obtained in two ways: first, using the hourglass vector \mathbf{h} in the computation of the stabilization term, and second, making use of the γ vector (31). The use of this vector results in an improvement in accuracy which is more marked as the distortion becomes more severe. In particular, whereas with the use of the hourglass vector the values of tip deflection at the bottom and top increase and decrease linearly, respectively, with an average value equal to the exact deflection, the use of the γ -vector leads to behaviour that is similar at the top and bottom, and that is furthermore a marginal improvement over that exhibited by the enhanced strain element Q1-E4 [14].

Example 2 (Cook's membrane problem). The Cook membrane problem is carried out as a plane strain example with nearly incompressible material behaviour ($E = 70$, $\nu = 0.4999$). Four different elements are compared in Fig. 4: the standard four-noded element Q1, the enhanced strain element Q1-E4, and the new element Q1EP with the use, respectively, of the hourglass vector and the γ -vector in the stabilization matrix.

The element showing the weakest performance is the standard Q1-element, even with an underintegrated volumetric part. The Q1-E4 and Q1EP with the γ -vector exhibit almost identical behaviour, while Q1EP with the use of the hourglass vector leads to behaviour that is slightly less accurate.

Example 3 (Plasticity). Here we investigate the Cook membrane problem again, for an elastic-plastic material. The total load is chosen to be 1.8 units, Young's modulus is equal to 70, and Poisson's ratio is 1/3.

Table 1
The Cook membrane problem: tip displacements for an elastic–plastic material

Number of elements per side	Q1-E4	Q1EP
2	0.6543	0.5527
4	1.1070	0.7166
8	2.1727	1.2745
16	2.3496	1.8390

We make use of the von Mises yield condition with yield stress 0.243 units and isotropic hardening parameter 0.135.

It can be seen in Table 1 that the results obtained using Q1EP are not as good as those obtained using the enhanced strain formulation. One of the reasons for this behaviour is that, in the stabilized equivalent parallelogram formulation, yielding occurs only if the center of the element yields, while the enhanced strain formulation shows plastic behaviour if yielding occurs at just one of the integration points. Nevertheless, the stabilization method compares well, taking into account that the formulation is inversion-free, and therefore much more efficient than the enhanced strain formulation.

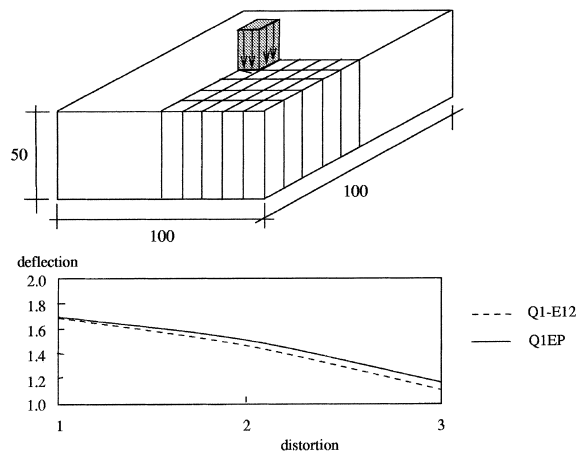


Fig. 5. The effect of distortion in three dimensions.

Table 2
Eigenvalues of the unit cube

Q1	Q1-E9	Q1-E12	Q1EP
0.30000D + 10	0.30000D + 10	0.30000D + 10	0.30000D + 10
0.66667D + 09	0.11111D + 09	0.20000D + 01	0.20000D + 01
0.66667D + 09	0.11111D + 09	0.20000D + 01	0.20000D + 01
0.66667D + 09	0.11111D + 09	0.20000D + 01	0.20000D + 01
0.11111D + 09	0.20000D + 01	0.20000D + 01	0.20000D + 01
0.11111D + 09	0.20000D + 01	0.20000D + 01	0.20000D + 01
0.11111D + 09	0.20000D + 01	0.20000D + 01	0.20000D + 01
0.20000D + 01	0.20000D + 01	0.20000D + 01	0.20000D + 01
0.20000D + 01	0.20000D + 01	0.20000D + 01	0.20000D + 01
0.20000D + 01	0.20000D + 01	0.20000D + 01	0.20000D + 01
0.20000D + 01	0.20000D + 01	1.33333D + 01	1.33333D + 01
0.20000D + 01	0.20000D + 01	0.66667D + 00	0.66667D + 00
0.20000D + 01	0.20000D + 01	0.66667D + 00	0.66667D + 00
0.13333D + 01	0.13333D + 01	0.66667D + 00	0.66667D + 00
0.10000D + 01	0.66667D + 00	0.66667D + 00	0.66667D + 00
0.10000D + 01	0.66667D + 00	0.66667D + 00	0.66667D + 00
0.10000D + 01	0.66667D + 00	0.66667D + 00	0.66667D + 00
0.33333D + 00	0.33333D + 00	0.33333D + 00	0.33333D + 00
0.33333D + 00	0.33333D + 00	0.33333D + 00	0.33333D + 00

4.2. Three-dimensional problems

Example 4 (*A cube with distorted elements*). The brick in Fig. 5 is clamped at its base and loaded as shown. The elements are randomly distorted, the measure of distortion ranging from 1, corresponding to no distortion, to 3. Young's modulus E is 2100 units, while a value of Poisson's ratio of 0.4999 ensures a condition of quasi-incompressibility. The total load is 1000 units.

The performances of the Q1-E12 [15] and Q1EP elements are very similar, though the latter performs slightly better with increasing distortion. Taking into account the economy in setting up the stiffness matrix for the equivalent parallelepiped, there is a clear advantage in using the Q1EP element.

Example 5 (*Eigenvalue analysis*). In this example an eigenvalue analysis is carried out along the lines of that reported in [15]. The eigenvalues of a unit cube with a ratio of bulk modulus to shear modulus of 10^9 are computed. Six zero eigenvalues are linked to rigid body modes, and are not given in Table 2, which contains details of the other eigenvalues.

The locking of the standard Q1 element is evident, while it can also be observed that the nine additional enhanced modes in element Q1-E9 are not sufficient in the nearly incompressible case. Element Q1-E9 exhibits four locking modes, while physically there is only volumetric locking mode. As expected, the fully integrated element Q1-E12 and Q1EP give identical results.

5. Conclusions

Motivated by the notion of the equivalent parallelogram and parallelepiped, and in particular by the property that they possess of being affine figures closest to a given quadrilateral or hexahedron, we have developed a new family of elements which have the properties of accuracy and economy. The accuracy of these elements derives from their close association with the elements based on incompatible modes, while their economy is based on the fact that only a single integration point is used per element. In this respect, the elements closely resemble those based on underintegration coupled with stabilization, with the important property that the stabilization matrices can be evaluated in closed form. The error due to the replacement of the original element by its equivalent affine figure is of the order of mesh size, so that the order of the error due to the finite element approximation is not adversely affected by this modification.

In the traditional incompatible modes or enhanced strain methods, accuracy decreases with an increase in distortion. For the elements presented here the sensitivity to distortion is less pronounced. The element is easily adapted to use in problems of elastoplasticity, while the extension to problems of finite strain elasticity is studied in [12] in the context of plane problems, and in [13] for three-dimensional problems.

Acknowledgements

The work was supported by the Foundation for Research Development; this support is gratefully acknowledged.

Appendix A

In the following the stabilization factors ϵ_i are given for the general case of a fully occupied symmetric material matrix for 2D problems; a , b and d represent the given geometrical properties of the parallelogram before the rotation to the physical axes, while e_{ij} represents the data of the material matrix of line i and column j .

$$\begin{aligned} \epsilon_1 = & \frac{1}{\kappa_1} \frac{4}{3} (b^4 e_{13}^4 e_{22} - 2b e_{13}^3 (d^2 e_{22} (-de_{22}) + b e_{23}) + b^2 e_{12} (d e_{22} + b e_{23})) + d^2 e_{12}^2 e_{33} (b^2 e_{12}^2 - 2b d e_{12} e_{23} \\ & + a^2 e_{23}^2 + d^2 e_{23}^2 + 2b^2 e_{12} e_{33} - a^2 e_{22} e_{33} - d^2 e_{22} e_{33}) + b^2 e_{11}^2 (-d^2 e_{22} e_{23}^2) + 2b d e_{23}^3 \\ & + d^2 e_{22}^2 e_{33} - 2b d e_{22} e_{23} e_{33} - b^2 e_{23}^2 e_{33} + b^2 e_{22} e_{23}^2) + e_{11} (b^2 d^2 e_{12}^2 e_{23}^2 - 2b d^3 e_{12} e_{23}^3 + a^2 d^2 e_{23}^4 \\ & + d^4 e_{23}^4 - 2b^2 d^2 e_{12}^2 e_{22} e_{33} + 2b^3 d e_{12}^2 e_{23} e_{33} + 2b d^3 e_{12} e_{22} e_{23} e_{33} + 2b^2 d^2 e_{12} e_{23}^2 e_{33} \\ & - 2a^2 d^2 e_{22} e_{23}^2 e_{33} - 2d^4 e_{22} e_{23}^2 e_{33} - b^4 e_{12}^2 e_{33}^2 - 2b^2 d^2 e_{12} e_{22} e_{23}^2 + a^2 d^2 e_{22}^2 e_{33}^2 \\ & + d^4 e_{22}^2 e_{33}^2) + e_{13}^2 (b^2 d^2 e_{12}^2 e_{22} + 4b^3 d e_{12}^2 e_{23} - 6b d^3 e_{12} e_{22} e_{23} + 4b^2 d^2 e_{12} e_{23}^2 + a^2 d^2 e_{22} e_{23}^2 \\ & + d^4 e_{22} e_{23}^2 + b^4 e_{12}^2 e_{33} + 2b^2 d^2 e_{12} e_{22} e_{33} - a^2 d^2 e_{22}^2 e_{33} - d^4 e_{22}^2 e_{33} + b^2 e_{11} (-d^2 e_{22}^2) \\ & + 2b d e_{22} e_{23} + b^2 e_{23}^2 - 2b^2 e_{22} e_{33})) - 2e_{13} (-b e_{11} (b d^2 e_{12} e_{22} e_{23} - 3b^2 d e_{12} e_{23}^2 + d^3 e_{22} e_{23}^2 \\ & - b d^2 e_{23}^3 + b^2 d e_{12} e_{22} e_{33} - d^3 e_{22}^2 e_{33} + b^3 e_{12} e_{23} e_{33} + b d^2 e_{22} e_{23} e_{33})) + d e_{12} (b^2 d e_{12}^2 e_{23} \\ & - 2b d^2 e_{12} e_{23}^2 + a^2 d e_{23}^3 + d^3 e_{23}^3 + b^3 e_{12}^2 e_{33} - b d^2 e_{12} e_{22} e_{33} + 3b^2 d e_{12} e_{23} e_{33} - a^2 d e_{22} e_{23} e_{33} - d^3 e_{22} e_{23} e_{33})), \end{aligned}$$

$$\begin{aligned} \kappa_1 = & a^2 (e_{23}^2 - e_{22} e_{33}) (b^4 e_{13}^2 - 2b d e_{13} (b^2 e_{12} + d (-de_{22}) + b e_{23})) - b^2 e_{11} (d^2 e_{22} - 2b d e_{23} + b^2 e_{33}) \\ & + d^2 (b^2 e_{12}^2 - 2b d e_{12} e_{23} + d^2 e_{23}^2 + 2b^2 e_{12} e_{33} - d^2 e_{22} e_{33}), \end{aligned}$$

$$\epsilon_3 = \frac{1}{\kappa_3} \frac{4}{3} b^2 (e_{13}^2 e_{22} - 2e_{12} e_{13} e_{23} + e_{12}^2 e_{33} + e_{11} (e_{23}^2 - e_{22} e_{33})),$$

$$\begin{aligned} \kappa_3 = & b^4 e_{13}^2 - 2b d e_{13} (b^2 e_{12} + d (-de_{22}) + b e_{23}) - b^2 e_{11} (d^2 e_{22} - 2b d e_{23} + b^2 e_{33}) + d^2 (b^2 e_{12}^2 \\ & - 2b d e_{12} e_{23} + d^2 e_{23}^2 + 2b^2 e_{12} e_{33} - d^2 e_{22} e_{33}), \end{aligned}$$

$$\epsilon_2 = \frac{d}{b} \epsilon_3.$$

References

- [1] U. Andelfinger, E. Ramm, EAS-elements for two-dimensional, three-dimensional, plate and shell structures and their equivalence to HR-elements, *International Journal for Numerical Methods in Engineering* 36 (1993) 1311–1337.
- [2] K. Arunakirinathar, B.D. Reddy, Some geometrical results and estimates for quadrilateral finite elements, *Computer Methods in Applied Mechanics and Engineering* 122 (1995) 307–314.
- [3] K. Arunakirinathar, B.D. Reddy, Further results for enhanced strain methods with isoparametric elements, *Computer Methods in Applied Mechanics and Engineering* 127 (1995) 127–143.
- [4] T. Belytschko, J.S.-J. Ong, W.K. Liu, J.M. Kennedy, Hourglass control in linear and nonlinear problems, *Computer Methods in Applied Mechanics and Engineering* 43 (1984) 251–276.
- [5] T. Belytschko, W. Bachrach, Efficient implementation of quadrilaterals with high coarse-mesh accuracy, *Computer Methods in Applied Mechanics and Engineering* 54 (1986) 279–301.
- [6] D.P. Flanagan, T. Belytschko, A uniform strain hexahedron and quadrilateral with orthogonal hourglass control, *International Journal for Numerical Methods in Engineering* 17 (1981) 679–706.
- [7] W.L. Hacker, H.L. Schreyer, Eigenvalue analysis of compatible and incompatible rectangular four-node quadrilateral elements, *International Journal for Numerical Methods in Engineering* 28 (1989) 687–703.
- [8] U. Hueck, B.D. Reddy, P. Wriggers, On the stabilization of the rectangular four-node quadrilateral element, *Communications in Numerical Methods in Engineering* 10 (1994) 555–563.
- [9] T.H.H. Pian, K. Sumihara, Rational approach for assumed stress finite elements, *International Journal for Numerical Methods in Engineering* 20 (1984) 1685–1695.
- [10] B.D. Reddy, M. Küssner, The four-noded quadrilateral with a 2×1 integration rule: application to plates and other problems, *Computer Methods in Applied Mechanics and Engineering* 149 (1997) 101–112.
- [11] B.D. Reddy, J.C. Simo, Stability and convergence of a class of enhanced strain methods, *SIAM Journal on Numerical Analysis* 32 (1995) 1705–1728.
- [12] S. Reese, M. Küssner, B.D. Reddy, A new stabilization technique for finite elements in nonlinear elasticity, *International Journal for Numerical Methods in Engineering* 44 (1999) 1617–1652.

- [13] S. Reese, P. Wriggers, B.D. Reddy, A new locking-free brick element technique for large deformation problems in elasticity, *Computers and Structures* 75 (2000) 291–304.
- [14] J.C. Simo, S. Rifai, A class of mixed assumed strain methods and the method of incompatible modes, *International Journal for Numerical Methods in Engineering* 29 (1990) 1595–1638.
- [15] J.C. Simo, F. Armero, R.L. Taylor, Improved version of assumed enhanced strain tri-linear elements for 3D finite deformation problems, *Computer Methods in Applied mechanics and Engineering* 110 (1993) 359–366.
- [16] R.L. Taylor, P.J. Beresford, E.L. Wilson, A non-conforming element for stress analysis, *International Journal for Numerical Methods in Engineering* 10 (1976) 1211–1220.
- [17] E.L. Wilson, R.L. Taylor et al., Incompatible displacement models, in: *Numerical and Computer Models in Structural Mechanics*, Academic Press, New York, 1973.